Artificial neural network method for determining optical properties from double-integrating-spheres measurements

Chenxi Li (李晨曦)[1,2], Huijuan Zhao (赵会娟)[2*], Qiuyin Wang (王秋殷)[2], and Kexin Xu (徐可欣)[1,2]

[1]*State Key Laboratory of Precision Measuring Technology and Instruments, Tianjin University, Tianjin 300072, China*

[2]*College of Precision Instruments and Optoelectronics Engineering, Tianjin University, Tianjin 300072, China*

[*]*E-mail: huijuanzhao@tju.edu.cn*

Received April 13, 2009

Accurate measurement of the optical properties of biological tissue is very important for optical diagnosis and therapeutics. An artificial neural network (ANN)-based inverse reconstruction method is introduced to determine the optical properties of turbid media, which is based on the reflectance (R) and transmittance (T) of a thin sample measured by a double-integrating-spheres system. The accuracy and robustness of the method has been validated, and the results show that the root mean square errors (RMSEs) of the absorption coefficient μ_a and scattering coefficient μ'_s reconstruction are less than 0.01 cm^{-1} and 0.02 cm^{-1}, respectively. The algorithm is not only very accurate in the case of a lower albedo ($\sim$0.33), but also very robust to the noise of R and T especially for the μ'_s reconstruction.

OCIS codes: 120.3150, 300.1030, 290.5820, 290.7050.

doi: 10.3788/COL20100802.0173.

The determination of the optical properties of bidogical tissue is essential for both diagnostic and therapeutic applications. Different methods, such as the diffuse reflectance measurements in frequency-domain, time-domain, and spatially resolved steady-state[1−6], have been applied to determine the optical properties of tissue *in vivo*. Double-integrating-spheres (DIS) method has been widely adopted as the "gold standard" for determining the optical properties *in vitro*, because it is applicable for samples in different conditions with high accuracy[7]. The optical properties such as the absorption coefficient μ_a and reduced scattering coefficient μ'_s are determined by the measurements of the total reflectance (R) and transmittance (T) of a thin sample between the two spheres.

The accuracy of the optical properties measurements not only depends on the precision of the measuring system but also is affected by the limitation of the reconstruction algorithms. Several methods have been applied to solve the problem of extracting μ'_s and μ_a from the R and T measurements by DIS, e.g., the inverse adding-doubling (IAD) method and inverse Monte-Carlo (IMC) simulation. The limitations of the IAD method include the inability to account for the exact boundary conditions, the failure to describe the media of low albedo, and the instability in the reconstruction[8]. Although the IMC method is more accurate and suitable for a wide range of the optical properties measurement, but its calculation speed is slow, and it is more sensitive to the random noise of the Monte-Carlo simulation (MCS)[9,10].

In this letter, a primary method based on the artificial neural nets (ANN) is used to determine optical properties from the integrating sphere measurement of R and T on thin turbid biological samples. The ANN method has been widely utilized in the nonlinear mapping, prediction and modeling[11], as well as in extracting optical properties from the diffuse reflectance[1]. But to our knowledge, the combination of the ANN method to the DIS system has not been reported yet. Here, the developed method is verified with both the simulation and experimental processes. For the simulation process, firstly, ANN is trained with the data generated from the MCS; secondly, the algorithm is evaluated to reconstruct μ_a and μ'_s with the computed R and T from the MCS; and at last, the algorithm is compared with other calculation methods. For the experimental process, ANN is trained with the measured R and T under different optical properties, and the algorithm is then used to extract the optical properties of different samples.

All the experiments and simulations[10,12] are based on the system shown in Fig. 1. In the simulation, the sample and the glass slide are assumed to be a semi-infinite slab with the thicknesses d_{sample} = 0.7 mm and d_{slide} = 1 mm, respectively. The refractive index of the glass slides is assumed to be n_{slide} = 1.47. For each simulation, 1×10^7 photons were traced.

R and T of the sample were measured in the wavelength of 633 nm using the relative measurement method. The values of R and T can be calculated according to[7]

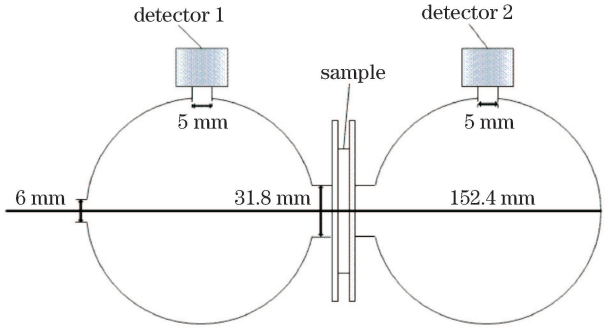

Fig. 1. DIS setup for the measurements of R_{meas} and T_{meas}.

$$R = \frac{(V_{m1} - V_{n1})r_{ref}}{V_{01} - V_{pn1}} \quad , \quad T = \frac{V_{m2} - V_{n2}}{V_{02} - V_{pn2}} \quad , \qquad (1)$$

where V_{01} and V_{02} are the detected light power for sphere 1 and 2 when the standard reflectance (transmittance) with a reflectivity (transmittance) of r_{ref} ($t_{ref} = 1$) is measured, respectively. V_{m1} and V_{m2} are the reflected and transmitted light power from detector 1 and 2, respectively, when the sample is measured. $V_{pn,x}$ and $V_{n,x}$ ($x \in 1, 2$) are the noise caused by the scattered light in the xth detector with and without light passing through the spheres, respectively. The measured R_{meas} and T_{meas} are then used to extract μ_a and μ_s' with the inverse algorithm.

When the ANN method was applied to extract the optical properties from R and T, a continuous mapping of R and T to [μ_a, μ_s'] was required. We generated a 16×41 matrices of R_{sim} and T_{sim} using the MCS[10] in the following typical ranges of biological optical properties:

$$0.5\ \text{cm}^{-1} \le \mu_a \le 2\ \text{cm}^{-1}, 10\ \text{cm}^{-1} \le \mu_s' \le 50\ \text{cm}^{-1},$$
$$g = 0.7, n = 1.34, \qquad (2)$$

where g is the anisotropy factor. The results of R, T, radically distributions of the diffuse R and T were recorded. According to the principle and geometry of the integrating sphere, the photons exited beyond the range of the sample port and the cross talk between the two spheres would deduct from R and T. It should be noted that R_{sim} here included both specular and diffuse reflectance, while T_{sim} included collimated and diffuse transmittance. The mapping of [μ_a, μ_s'] onto R_{sim} and T_{sim} is shown in Fig. 2. From the figure, we can get that the R_{sim} and T_{sim} vary smoothly and continuously with (μ_a, μ_s').

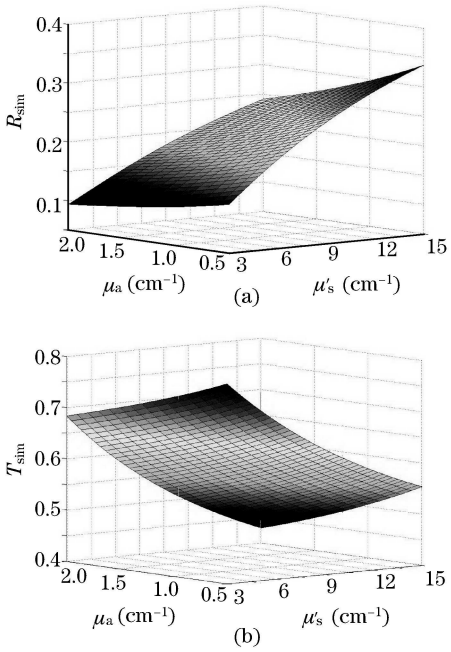

Fig. 2. (a) Total reflectance R and (b) transmittance T as a function of μ_a and μ_s' for a thin slab generated with the MCS.

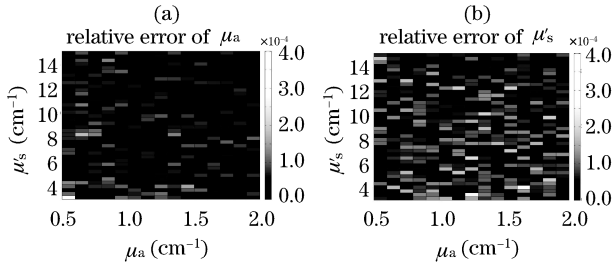

Fig. 3. The relative fitting errors of (a) μ_a and (b) μ_s'.

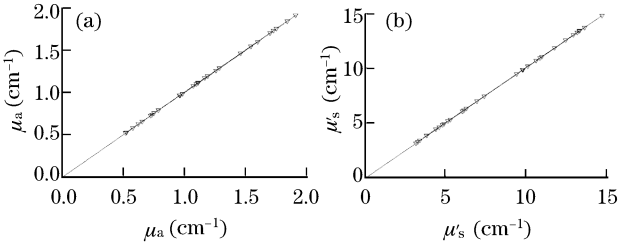

Fig. 4. Prediction accuracy of (a) μ_a and (b) μ_s' by using the BPNN method. '−' indicats the true values and '∇' indicats the predicted values.

The back propagation neural network (BPNN) model was applied to reconstruct μ_a and μ'_s, which includes two hidden layer nodes beside the input and output nodes. For a set of examples (input x_i ($x_i \in S^n$) and output y_i ($y_i \in S^m$)), there was a mapping h, in which $h(x_i) = y_i$. The net was trained with the calibration dataset to find a mapping f that was the best approximation to h. Two parameters, the learning rate and the transfer function, controled the BPNN process. The learning rate scaled the magnitude of the step down the error surface after each complete calculation in the network, and the transfer function finished the transform between the input and output[11].

The BPNN was trained by the dataset with the input dataset of (R_{sim}, T_{sim}) and output dataset (μ_a, μ_s') (in the range of (0.5 cm^{-1} ≤μ_a ≤ 2 cm^{-1}, 3 cm^{-1} ≤μ'_s ≤ 15 cm^{-1}), generated by the MCS. In the following, the datasets used in training and testing the BPNN method are defined as the calibration and validation datasets, respectively.

To test the fitting errors of the BPNN algorithm, we used the training dataset as the validation dataset, and defined the relative error of prediction as

$$f_{err} = \left| \frac{\mu_{pred} - \mu_{true}}{\mu_{true}} \right| \times 100\%. \qquad (3)$$

The results, as illustrated in Fig. 3, show that the f_{err} of μ_a is comparatively less than that of μ_s', and in the most points the relative error is below 0.01%. The results indicate that after the BPNN is well trained, it is accurate in fitting. The reasons for the big errors in μ_a and/or μ_s' may attribute to the random noise of the MCS.

To evaluate the accuracy of the BPNN method, a dataset of (μ_a, μ_s') was generated randomly from Matlab and regarded as the true values. Based on the dataset of (μ_a, μ_s') , (R_{sim}, T_{sim}) were then generated from the MCS and applied as the input of the BPNN method.

Table 1 Evaluation of the Optical Property Reconstruction Algorithm Based on the BPNN

Case	Calibration Datasets	Validation Datasets	RMSE in μ_a (cm^{-1})	RMSE in μ'_s (cm^{-1})
1	U	S without Noise	0.0035	0.0072
2		R without Noise	0.0031	0.0065
3		S with Noise	0.0098	0.0189
4		R with Noise	0.0084	0.0141
5	R	U without Noise	0.0045	0.0069
6		S without Noise	0.00465	0.0049
7		U with Noise	0.0096	0.0156
8		S with Noise	0.0082	0.0134

(S: self-validation; R: random; U: uniform)

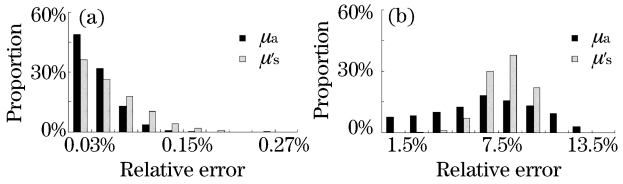

Fig. 5. Histogram of the relative errors by using (a) the BPNN and (b) IAD methods in the situation of $0.83 \ll a \ll 0.99$.

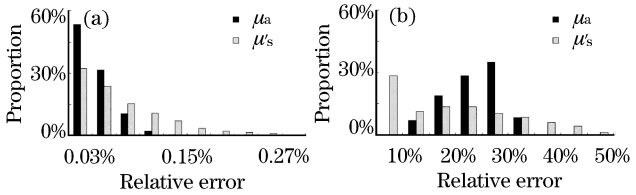

Fig. 6. Histogram of the relative errors by (a) the BPNN and (b) IAD methods in the situation of $0.33 \ll a \ll 0.90$.

As shown in Fig. 4, the predicted results are coincided with the true values very well, and the prediction errors of μ_a and μ'_s are both less than 0.15%.

The robustness of the BPNN method was also assessed by the calibration datasets and validation datasets. Two calibration-validation dataset pairs of R and T were generated from the MCS with the uniform and random (μ_a, μ'_s), respectively. In addition to the above validation datasets, 1% random noise was also added to R and T in the validation dataset and thus other two validation datasets were formed. The noise level of 1% was selected according to the signal-to-noise ratio (SNR) of the DIS system used in this letter (the SNR of the measuring system was about 0.5%) and other possible noise such as the variations cased by the samples. The prediction error for each calibration-validation pair was quantified using the root mean square error (RMSE)

$$f_{\mathrm{RMSE}} = \left[\frac{1}{m}\sum_{i=1}^{m}\left(\mu_{\mathrm{pred,i}} - \mu_{\mathrm{true,i}}\right)^2\right]^{1/2}, \qquad (4)$$

where m indicates the total number of data in a dataset.

The results summarized in Table 1 show that the RMSEs in the μ_a and μ'_s reconstruction are less than 0.005 cm^{-1} and 0.008 cm^{-1} without noise in R and T. When the noise is added, the RMSEs are a little bigger but still less than 0.01 cm^{-1} and 0.02 cm^{-1} for the μ_a and μ'_s reconstruction, respectively, which indicate that the BPNN method is robust to noise.

The performances of the BPNN method were compared with that of the IAD method in both the ability to reconstruct optical properties in the case of lower albedo ($a = 0.33 - 0.90$) and the robustness to noise[7].

It is well known that IAD is noneffective for the low albedo samples[8]. For one of the simulation dataset, μ_a was big enough to get a small albedo. Dataset 1 was for the higher albedo $0.83 \leqq a \leqq 0.99$ ($0.5\ cm^{-1} \leqq \mu_a \leqq 2\ cm^{-1}$, $10\ cm^{-1} \leqq \mu'_s \leqq 50\ cm^{-1}$), while Dataset 2 for lower albedo $0.33 \leqq a \leqq 0.90$ ($5\ cm^{-1} \leqq \mu_a \leqq 20\ cm^{-1}$, $10\ cm^{-1} \leqq \mu'_s \leqq 50\ cm^{-1}$). With an increment of 0.1 cm^{-1} and 1 cm^{-1} for μ_a in the dataset 1 and 2 respectively, and an increment of 1 cm^{-1} for μ'_s in both datasets, each dataset included 656 samples. For every couple of μ_a and μ'_s in a dataset, R and T were then generated with the MCS and treated as the input to the BPNN and IAD method for reconstructing μ_a and μ'_s. The two methods were compared by a measure named proportion which is the percentage of the total 656 samples with a reconstruction relative error.

As it can be seen from Figs. 5 and 6, the mean relative errors in the reconstruction of μ_a and μ'_s are about 3.26×10^{-2}% and 6.61×10^{-2}% for lower albedo, and about 3.6×10^{-2}% and 5.8×10^{-2}% for higher albedo. The results indicate that the reconstruction accuracy by the BPNN method is almost the same for the lower and higher albedo. However, for the IAD method, the mean relative errors in the reconstruction of μ_a and μ'_s are about 6% and 9% for higher albedo, but 23.4% and 19% for lower albedo. It is thus concluded that the BPNN method is much more accurate than the IAD method especially in lower albedo region.

The 1% random noise was then added to R and T in dataset 1 to compare the robustness of the two methods. Results show that the two methods have a comparable robustness in reconstructing μ_a (results are not shown here). However, as illustrated in Fig. 7, in the case of adding the noise, the BPNN method can provide more

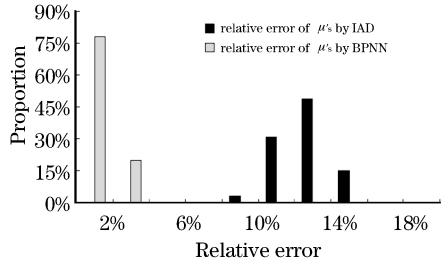

Fig. 7. The relative errors of the μ_s' reconstruction by using the BPNN and IAD methods with 1% noise added to R and T.

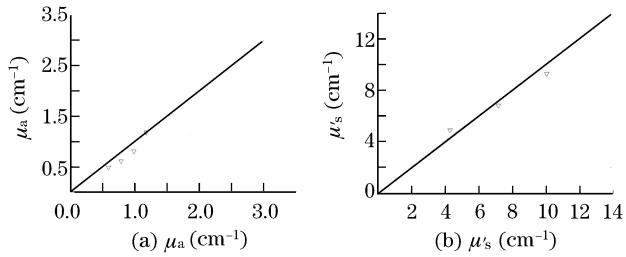

Fig. 8. Reconstructed (∇) (a) μ_a and (b) μ_s' by the BPNN algorithm from the experimental data.

accurate μ_s' reconstruction than the IAD method does.

The developed algorithm was also evaluated with the phantom measurements. The solution of Intralipid-10% and Indian Ink were used as the scattering and absorption ingredient, respectively. Assuming that the scattering due to the Indian Ink was negligible, we determined the "true" μ_a of the Indian Ink solution from the collimated transmittance measurement using a spectrometer (HR2000, Ocean Optics Co. Ltd). The "true" μ'_s of the Intralipid-10% was calculated by Mie theory[12].

The 4×4 μ_a and μ'_s pairs (μ_a = 0.5, 1, 1.5, and 2 cm^{-1}, μ_s' = 3, 6, 9, and 12 cm^{-1}) were selected as the calibration datasets. The R_{meas} and T_{meas} of the calibration datasets were measured by the DIS system, and then $\{[\mu_a, \mu'_s]\ , [R_{meas}, T_{meas}]\}$ was applied to train the BPNN. To evaluate the BPNN algorithm, different phantoms were compounded and measured. The optical property was reconstructed with the well trained BPNN. As shown in Fig. 8, the mean relative error for the reconstruction of μ_a and μ_s' are within the range of 5% and 2%.

In conclusion, the developed algorithm for extracting optical properties from the measurements of R and T of the DIS system is dealt with, which is based on the artificial neural networks. The simulations results show that, with the algorithm, the RMSEs in the μ_a and μ_s' reconstruction are less than 0.01 cm^{-1} and 0.02 cm^{-1}. Compared with the IAD method, the algorithm is not only more accurate for the lower albedo cases but also more robust to the noise of R and T especially for the μ_s' reconstruction. The experimental results also demonstrate that the effectiveness of the algorithm in reconstructing optical properties with the measurement data from the DIS system. In short, it is evident that, once the calibration model has been implemented, the developed algorithm is more suitable to the real-time reconstruction of optical property from the DIS system.

This work was supported by the National Natural Science Foundation of China (No. 30870657), the Natural Science Foundation of Tianjin (No. 09JCZDJC18200), and the 111 Project (No. B07014).

References

1. T. J. Pfefer, L. S. Matchette, C. L. Bennett, J. A. Gall, and J. N. Wilke, J. Biomed. Opt. **8,** 2 (2003).
2. G. M. Palmer and N. Ramanujam, Appl. Opt. **45,** 5 (2006).
3. H. Zhao, X. Zhou, J. Liang, and S. Zhang, Chin. Opt. Lett. **6,** 12 (2008).
4. F. Gao, L. Zhang, J. Li, and H. Zhao, Chin. Opt. Lett. **6,** 12 (2008).
5. A. Kienle, M. S. Patterson, R. Bays, G. Wagnieres, and H. Bergh, Appl. Opt. **37,** 4 (1998).
6. N. Rajaram, T. H. Nguyen, and J. W. Tunnell. J. Biomed. Opt. **13,** 5 (2008).
7. J. W. Pickering, S. A. Prahl, N. V. Wieringen, J. F. Beek, H. J. C. M. Sterenborg, and M. J. C. van Gemert, Appl. Opt. **32,** 4 (1993).
8. D. Zhu, W. Lu, S. Zeng, and Q. Luo, J. Biomed. Opt. **12,** 6 (2007).
9. J. S. Dam, T. Dalgaard, P. E. Fabricius, and S. A. Engels, Appl. Opt. **39,** 7 (2000).
10. L. Wang, S. L. Jacques, and L. Zheng, Comput. Meth. Programs Biomed. **47,** 131 (1995).
11. J. S. Judd and J. Stephen, *Neural Network Design and the Complexity of Learning* (The MIT Press, Cambridge, 1990).
12. H. J. van Staveren, C. J. M. Moes, J. van Marle, S. A. Prahl, and M. J. C. van Gemert, Appl. Opt. **30,** 31 (1991).